





OPEN

Synergistic chemo-photothermal therapy using gold nanorods supported on thiol-functionalized mesoporous silica for lung cancer treatment

Maryam Deinavizadeh¹, Ali Reza Kiasat^{1,2}, Mohammad Shafiei³, Mohammad Sabaeian^{4,5}, Roya Mirzajani¹, Seyed Mohammadsaleh Zahraei³, Fateme Khalili¹, Minmin Shao⁶, Aimin Wu⁷, Pooyan Makvandi^{8,9} & Nasrin Hooshmand¹⁰

Cancer therapy necessitates the development of novel and effective treatment modalities to combat the complexity of this disease. In this project, we propose a synergistic approach by combining chemo-photothermal treatment using gold nanorods (AuNRs) supported on thiol-functionalized mesoporous silica, offering a promising solution for enhanced lung cancer therapy. To begin, mesoporous MCM-41 was synthesized using a surfactant-templated sol-gel method, chosen for its desirable porous structure, excellent biocompatibility, and non-toxic properties. Further, thiol-functionalized MCM-41 was achieved through a simple grafting process, enabling the subsequent synthesis of AuNRs supported on thiol-functionalized MCM-41 (AuNR@S-MCM-41) via a gold-thiol interaction. The nanocomposite was then loaded with the anticancer drug doxorubicin (DOX), resulting in AuNR@S-MCM-41-DOX. Remarkably, the nanocomposite exhibited pH/NIR dual-responsive drug release behaviors, facilitating targeted drug delivery. In addition, it demonstrated exceptional biocompatibility and efficient internalization into A549 lung cancer cells. Notably, the combined photothermal-chemo therapy by AuNR@S-MCM-41-DOX exhibited superior efficacy in killing cancer cells compared to single chemo- or photothermal therapies. This study showcases the potential of the AuNR@S-MCM-41-DOX nanocomposite as a promising candidate for combined chemo-photothermal therapy in lung cancer treatment. The innovative integration of gold nanorods, thiol-functionalized mesoporous silica, and pH/NIR dual-responsive drug release provides a comprehensive and effective therapeutic approach for improved outcomes in lung cancer therapy. Future advancements based on this strategy hold promise for addressing the challenges posed by cancer and transforming patient care.

Keywords Chemo-photothermal therapy, Chemotherapy, Photothermal therapy, Gold Nanorods, Cancer Cells, Doxorubicin, Dual-responsive, Lung cancer cells, Mesoporous Silica MCM-41

¹Department of Chemistry, Faculty of Science, Shahid Chamran University of Ahvaz, Ahvaz, Iran. ²Petroleum Geology and Geochemistry Research Center (PGGRC), Shahid Chamran University of Ahvaz, Ahvaz, Iran. ³Department of Biology, Faculty of Science, Shahid Chamran University of Ahvaz, Ahvaz, Iran. ⁴Department of Physics, Faculty of Science, Shahid Chamran University of Ahvaz, Ahvaz, Iran. ⁵Center for Research On Laser and Plasma, Shahid Chamran University of Ahvaz, Ahvaz, Iran. ⁶Department of Otorhinolaryngology, The Second Affiliated Hospital of Shanghai University, Wenzhou Central Hospital, Wenzhou, China. ⁷Department of Orthopaedics, Key Laboratory of Structural Malformations in Children of Zhejiang Province, Key Laboratory of Orthopaedics of Zhejiang Province, The Second Affiliated Hospital and Yuying Children's Hospital of Wenzhou Medical University, Wenzhou 325000, Zhejiang, China. ⁸Centre of Research Impact and Outcome, Chitkara University, Rajpura 140401, Punjab, India. ⁹Department of Biomaterials, Saveetha Dental College and Hospitals, SIMATS, Saveetha University, Saveetha University, Chennai 600077, India. ¹⁰Laser Dynamics Laboratory, School of Chemistry and Biochemistry, Georgia Institute of Technology, Atlanta, GA 30332, USA. ✉email: akiasat@scu.ac.ir; pooyanmakvandi@gmail.com; nhooshmand3@gatech.edu

Cancer, a complex and devastating disease, requires innovative therapeutic strategies that can effectively target tumor cells while minimizing adverse effects on healthy tissues^{1–3}. Photothermal therapy (PTT) is a highly selective and noninvasive therapeutic technique that has shown great promise for the treatment of cancer⁴. Nowadays, various nanoscale materials have been widely explored as photothermal agents (PTAs).

Among these nanomaterials, gold-based nanoarchitectures (e.g., nanorods, nanostars, nanocages, nanospheres and nanoshells) have been extensively studied as PTAs due to their tunable localized surface plasmon resonance (LSPR) properties^{5–7}, low toxicity and excellent biocompatibility^{8,9}. Gold nanorods (GNRs) are particularly interesting for concurrent cancer therapy due to their unique properties such as their excellent biocompatibility, controllable size, tunable surface plasmon resonance (SPR)¹⁰, high photothermal conversion efficiency and ease of surface modification^{11–13}. However, AuNRs can aggregate in the tumor microenvironment which reduces their optical attributes and diminishes the photothermal therapy efficacy¹⁴. Thus, surface modification of AuNRs by non-toxic and biocompatible stabilizers is necessary to improve their stability and PTT efficacy^{15–19}.

Photothermal therapy using photothermal agents alone has limitations in completely destroying cancer cells²⁰. Light penetration into deeper tumor tissues is reduced due to absorption and scattering, leading to decreased photothermal therapy efficiency²¹. Researchers have combined PTT with additional therapeutic strategies to dominate these limitations and improve effectiveness^{22–26}. Among various combination techniques, co-delivering anticancer drugs with photothermal agents has emerged as a highly promising approach. In this combination photothermal chemotherapy, the photothermal agent enables localized heating while the anticancer drug provides cytotoxic effects^{27–31}. Various materials were conjugated to gold nanorods (AuNRs) to enable drug loading for combination photothermal chemotherapy, including cell membrane coatings. These materials can target cancer cells specifically, deliver therapeutic agents to the tumor location, and induce hyperthermia to increase the therapeutic effect^{32,33}.

Mesoporous silica nanoparticles feature a variety of advantages, including simple surface modification, good biocompatibility and great chemical and mechanical stability³⁴.

Among the family of mesoporous silica nanoparticles, MCM-41 (Mobil Composition of Matter No. 41) possesses promising characteristics, instance e.g., having hexagonally shaped pores, an ordered mesoporous structure, enormous surface area (about 900–1500 m² g⁻¹) along with a narrow pore size distribution (2–10 nm)^{35–37}. Furthermore, the presence of a large number of silanol groups (Si–OH) on the surface MCM-41 simplifies functionalization of MCM-41, and the pore size can be appropriate for encapsulation of bioactive molecules^{38–41}. Furthermore, synergetic pH/NIR responsive drug delivery systems have been shown to be a promising strategy for selectively delivering anticancer drugs in tumors. These systems improve permeability and uptake of the targeted cells, as a result ameliorate the effectiveness of chemotherapy. Besides, these nanoscale materials can generate the hyperthermia under NIR laser to destroy tumor cells; this offers combined photothermal and chemotherapy^{42–45}.

By keeping these facts in mind and in continuing our research on the development of pH/NIR dual-responsive drug delivery using AuNRs@DOX for combined chemo-photothermal therapy^{46–48}, in this work, we developed AuNRs supported on thiol-MCM-41 (AuNR@S-MCM-41) as a drug support and designed the AuNR@S-MCM-41-DOX nanocomposite for controlled release of bioactive molecules and synergetic photothermal and chemotherapy techniques. First, gold nanorods were supported on thiolated MCM-41 via Au–S bonds (AuNR@S-MCM-41). Then, the anticancer drug doxorubicin (DOX) was loaded into the AuNR@S-MCM-41 nanocomposite by strong electrostatic interactions. Under near-infrared irradiation, we expected the AuNR@S-MCM-41-DOX nanocomposite to exhibit pH/NIR dual-responsive drug release behaviors and improve the efficacy of chemo-photothermal therapy compared to single therapy. The results of *in vitro* experiments conducted in this study showed that AuNR@S-MCM-41-DOX is both biocompatible and effective against A549 lung cancer cells. Overall, the nanocomposite demonstrated stimuli-responsive drug delivery performance, in which release is facilitated by internal and external triggers (e.g., tumor microenvironment and NIR laser).

Experimental section

Generals

Cetyltrimethylammonium bromide (CTAB), sodium borohydride (NaBH₄), L-ascorbic acid, Silver Nitrate (AgNO₃), Gold (III) chloride solution (HAuCl₄·3H₂O), [3-(4,5-dimethylthiazol-2-yl)-3,5-diphenyltetrazolium bromide] (MTT), tetraethylorthosilicate (TEOS), (3-mercaptopropyl)trimethoxy-silane (MPTMS), sodium hydroxide (NaOH), ethanol (EtOH), toluene, and hydrochloric acid (HCl) were purchased from Sigma-Aldrich. Doxorubicin hydrochloride (DOX) as an anti-cancer drug was obtained from Fenghua Lianbo. Co (Peking, China). Deionized water was used in all the experiments. Human lung cancer cell line A549 was obtained from the Pasteur Institute of Iran.

The absorbance of the AuNRs was measured using a UV-Vis spectrophotometer (TU-1901). To determine the size of the nanoparticles, a transmission electron microscope (TEM) (LEO-906E-80 kV) was used. Fourier transform infrared (FTIR) spectra were recorded using BOMEM MB-Series 1998 FT-IR spectrometer. To characterize the surface of the nanoparticles, a Zeta sizer Nano ZS instrument (Malvern Instruments, U.K.) was used to measure the surface zeta potentials. The An ICP-OES spectrometer (Optima 8300, Perkin Elmer) was used for determination of Au concentration in samples. Energy-dispersive X-ray spectroscopy (EDX) and EDX elemental mapping analysis were performed by FEI Tecnaï G2 F20S-TWIN at 200 kV. A continuous wave laser with wavelength 808 nm (GCSLS-05-7W00 fiber-coupled, Daheng Science and Technology, China) was used for the laser irradiation experiment (7 mm, 1.4 W, 3.6 W/cm²).

Photothermal performance

To evaluate the photothermal effect of the AuNR@S-MCM-41 nanocomposite, 100 μL of nanocomposite dispersions at various concentrations (0–25 nM) were added to a 96-well plate along with control wells. The control

sample was contained 100 μL of medium (DMEM) without any nanoparticle. Other wells contain nanoparticles with different concentrations. The plate was irradiated with a diode laser at 808 nm and a beam diameter of 7 mm, using a power density of 3.6 W/cm^2 for 5 min. The temperature of the solutions was measured using a thermocouple during laser irradiation.

Preparation of AuNR@S-MCM-41-DOX

A solution of DOX at a concentration of 5 μM (1 mL) was added to solution of AuNR@S-MCM-41 nanocomposite (5 mg, 5 mL) at a concentration of 228 nM in PBS buffer and stirred for 24 h at room temperature. The resulting AuNR@S-MCM-41-DOX was then separated and washed through centrifugation at 11,000 rpm for 10 min. The concentration of DOX in the supernatant solution was measured by a UV-Vis spectrometer at 485 nm. The efficiency percentages of DOX loading and entrapment were calculated using Eqs. (1) and (2), respectively.

$$DLE(\%) = \frac{(Total\ amount\ of\ DOX) - (Residual\ amount\ of\ DOX)}{(Total\ amount\ of\ Nanocomposite)} \times 100 \quad (1)$$

$$EE(\%) = \frac{Abs_{(original\ DOX)} - Abs_{(residual\ DOX)}}{Abs_{(original\ DOX)}} \times 100 \quad (2)$$

In vitro drug release performance of AuNR@S-MCM-41-DOX

In this experiment, a 5 mL dispersion of AuNR@S-MCM-41-DOX in PBS buffer was agitated at 130 rpm and 37 $^{\circ}\text{C}$ in the dark, with DOX concentration of 5 μM , at pH values of 5.5 or 7.4. After centrifuging the dispersions at various time intervals, the amount of released DOX in the supernatant was evaluated using a UV-Vis spectrometer at 485 nm. Additionally, DOX release was assessed under 808 nm laser irradiation (power density of 3.6 W cm^{-2}) in PBS with pH values of 5.5 and 7.4.

Results and discussion

Synthesis and characterization of AuNR@S-MCM-41-DOX

The preparation steps of AuNR@S-MCM-41-DOX nanocomposite as summarized in Scheme 1 are:

- A: synthesis of MCM-41 nanoparticles by surfactant-templated sol-gel method
- B: synthesis of MCM-41-SH via post grafting method using 3-mercaptopropyl trimethoxysilane
- C: preparation of AuNRs through seed-mediated growth method and assembly of MCM-41-SH on AuNRs via a gold-thiol interaction
- D: loading of DOX on AuNR@S-MCM-41 nanocomposite by strong electrostatic interactions

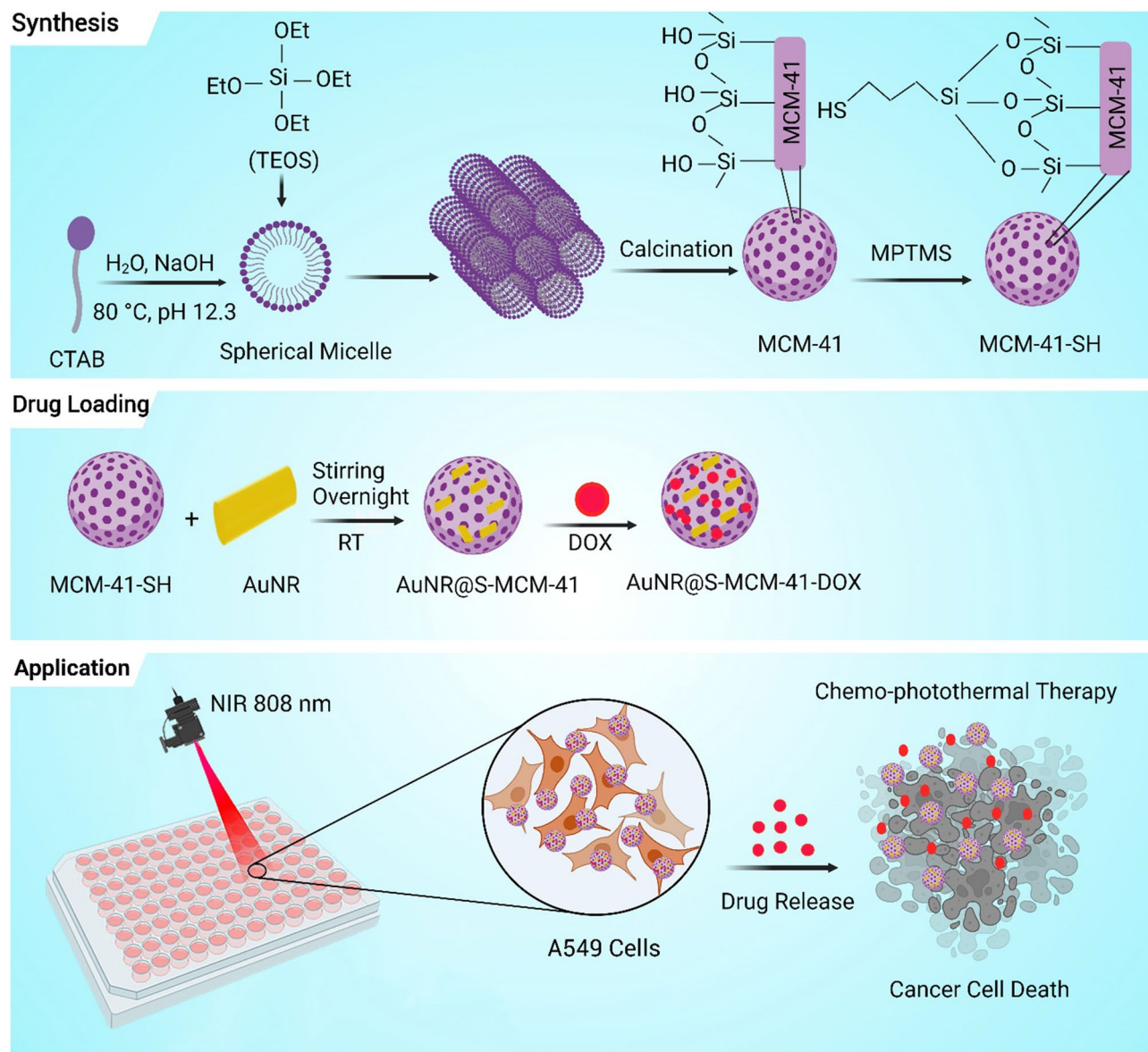
The successful synthesis of MCM-41-SH nanoparticles was confirmed by the FTIR spectra. The FTIR spectra of MCM-41 and MCM-41-SH are indicated in Fig. 1. The FTIR spectrum of MCM-41-SH (Fig. 1b) compared to that of MCM-41 (Fig. 1a) indicated the presence of the S-H stretching vibration in MCM-41-SH, which was confirmed by the detection of a weak vibrational band at 2583 cm^{-1} . This qualitative confirmation from the FTIR spectra displays that the thiol functional groups were successfully included into the MCM-41 nanoparticles⁴⁹.

The successful synthesis of AuNRs, AuNR@S-MCM-41, AuNR@S-MCM-41-DOX, and DOX was confirmed by FTIR spectra (Fig. 2A). The disappearance of the -SH absorption peak at 2583 cm^{-1} in AuNR@S-MCM-41 and AuNR@S-MCM-41-DOX confirms the formation of gold-sulfur covalent bonds. The FT-IR spectrum of DOX indicates two peaks at 1584 cm^{-1} and 1622 cm^{-1} (N-H) and one at 1725 cm^{-1} (C=O), which are also present but relatively weak in the FTIR spectrum of AuNR@S-MCM-41-DOX nanocomposite, confirming drug loading.

Also, the successful coating of AuNRs with MCM-41-SH and doxorubicin loading were verified through UV-Vis spectroscopy (Fig. 2B). AuNRs indicated transverse and longitudinal bands around 517 and 710 nm, respectively. The LSPR band was red shifted to nearly 748 nm on surface coating with MCM-41-SH, demonstrating the change in electronic conjugation following the chemical reaction and the Au-S bond formation, although the plasmon transverse band (519 nm) stayed approximately unchanged. Finally, successful loading of DOX in AuNR@S-MCM-41 was indicated by an LSPR to 760 nm.

The structure of AuNRs, AuNR@S-MCM-41, and AuNR@S-MCM-41-DOX were also analyzed by dynamic light scattering (DLS). The DLS measurements indicated that AuNRs, AuNR@S-MCM-41, and AuNR@S-MCM-41-DOX had hydrodynamic sizes about 54, 122.4 and 164.2 nm, respectively (Fig. 2C). The effect of hydrogen bonding between the amine and hydroxyl groups of DOX and the silanol hydroxyl groups of MCM-41 in the AuNRs@S-MCM-41-DOX nanocomposite, which produces aggregation, is the most likely the reason for the potential enhancement in the size of nanoparticles following loading of DOX.

The zeta potential of AuNRs in water (+39.2 mV) is likely the result of the presence of positively charged groups (CTAB) on the surface of the gold nanorods. When MCM-41-SH, which contains thiol groups, was used as a support for AuNRs, the zeta potential decreased to +29.8 mV. This decrease in zeta potential is probably due to the introduction of negatively charged functional groups (thiol). DOX loading onto the AuNR@S-MCM-41 nanocomposite further reduces the zeta potential to +25 mV. This decrease in zeta potential can be related to the interaction between the positively charged DOX molecules and the negatively charged functional groups on the surface of the nanocomposite, which leads to a decrease in the overall positive charge and thus a decrease in zeta potential (Fig. 2D).



Scheme 1. Schematic illustration for the synthesis of AuNR@S-MCM-41-DOX nanocomposite. CTAB: Cetyltrimethyl ammonium bromide, TEOS: Tetraethyl orthosilicate, MPTMS: (3-Mercaptopropyl) trimethoxysilane, DOX: Doxorubicin.

After synthesis and characterization of MCM-41-SH, gold nanorods were achieved by the seed-mediated growth method and their morphology was confirmed by TEM (Fig. 3A,B). The TEM images of more than 100 AuNRs were examined, and Image J software revealed that the average width and length of AuNRs were 11 ± 0.5 nm and 34 ± 2 nm, respectively, with an aspect ratio of 3.1 (Fig. 3G,H). Using ICP-OES, the concentration of Au atoms in AuNRs was calculated. Then, MCM-41-SH nanoparticles were applied as uniform and water-dispersible mesoporous structures as AuNR nanocarriers. The successfully prepared AuNR@S-MCM-41 nanocomposite was imaged by TEM (Fig. 3C,D). Finally, for the loading and delivery of the anticancer drug doxorubicin (DOX), AuNR@S-MCM-41 nanocomposite was utilized as a nanocarrier. The TEM images of the AuNR@S-MCM-41-DOX nanocomposite (Fig. 3E,F) confirm the loading of DOX in the AuNR@S-MCM-41 nanocomposite. The spatial distribution of Au, S, Si, and O on AuNR@S-MCM-41 was revealed via energy-dispersive X-ray spectroscopy (EDX) and elemental mapping further confirming that AuNR@S-MCM-41 nanocomposite was achieved (Fig. 3I–O).

Photothermal properties of AuNR@S-MCM-41

Near-infrared (NIR) light is a favorable source of light in photothermal therapy as it is transparent to biological systems and has sufficient tissue penetration depth. This can increase the photothermal (PT) efficiency of cancer cells by converting incident radiation into heat and reduce the side effects on normal cells⁵⁰. The photothermal properties of the AuNR@S-MCM-41 nanocomposite were studied by monitoring the temperature enhancement

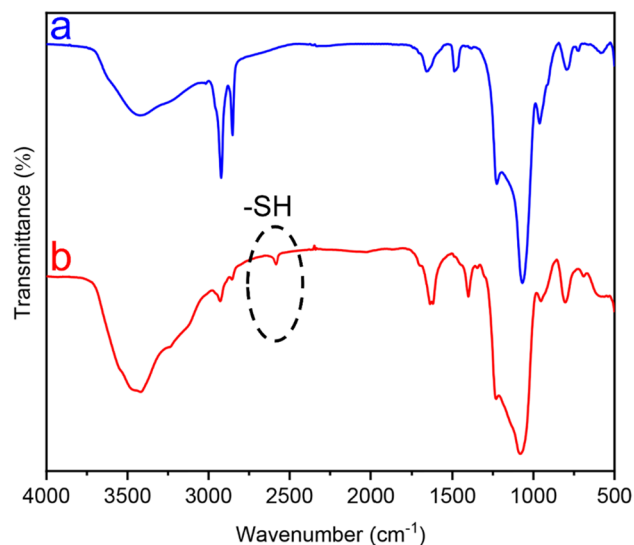


Figure 1. FTIR spectra of (a) MCM-41 and (b) MCM-41-SH.

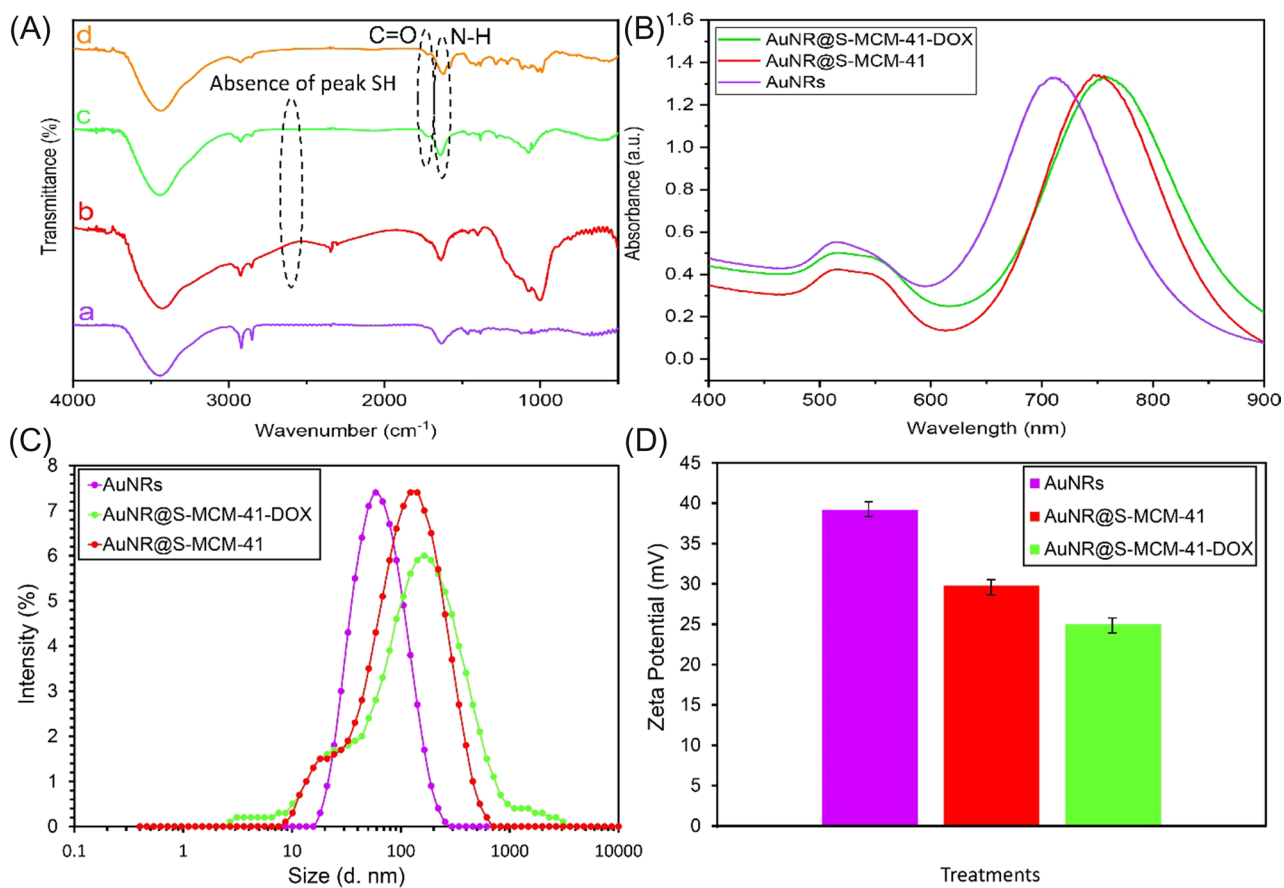


Figure 2. (A) FTIR spectra of AuNRs (a), AuNR@S-MCM-41 (b), AuNR@S-MCM-41-DOX (c), DOX (d); (B) the UV-Vis absorption spectra of AuNRs, AuNR@S-MCM-41 and AuNR@S-MCM-41-DOX; Hydrodynamic size analysis by DLS (C) and Surface zeta potential (D) of AuNRs, AuNR@S-MCM-41, and AuNR@S-MCM-41-DOX.

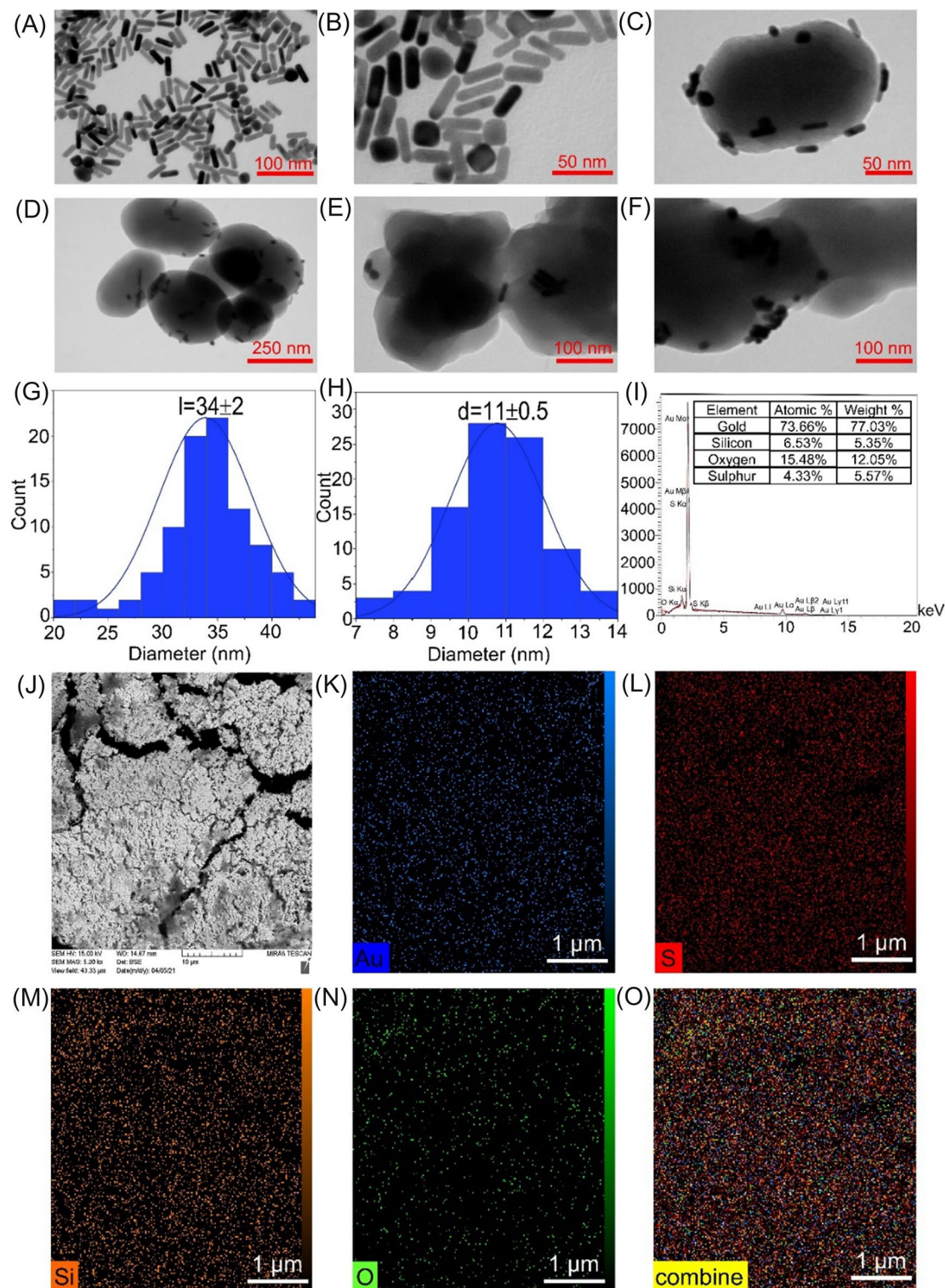


Figure 3. TEM images of (A), (B) AuNRs, (C), (D) AuNR@S-MCM-41, (E), (F) AuNR@S-MCM-41-DOX; (G), (H) Statistical data of length and diameter of more than 100 AuNRs as shown in (A), (B); (I) EDX and (J–O) SEM and EDX maps of AuNR@S-MCM-41, Au, S, Si, O and combined.

of the nanocomposite suspensions under 808 nm diode laser irradiation with a power density of 3.6 W/cm². The suspensions of AuNRs, AuNR@S-MCM-41 (with an equal concentration of 25 nM of AuNRs), and solutions of PBS and DOX were irradiated using the 808 laser. As displayed in Fig. 4A, the temperature of the AuNRs and AuNR@S-MCM-41 suspension increased from 24 to 63 °C and 24 to 56 °C after 5 min of irradiation, respectively. Meanwhile, the temperature of the PBS and DOX solutions did not significantly increase under the same conditions. These findings demonstrate that the AuNR@S-MCM-41 nanocomposite has remarkable potential

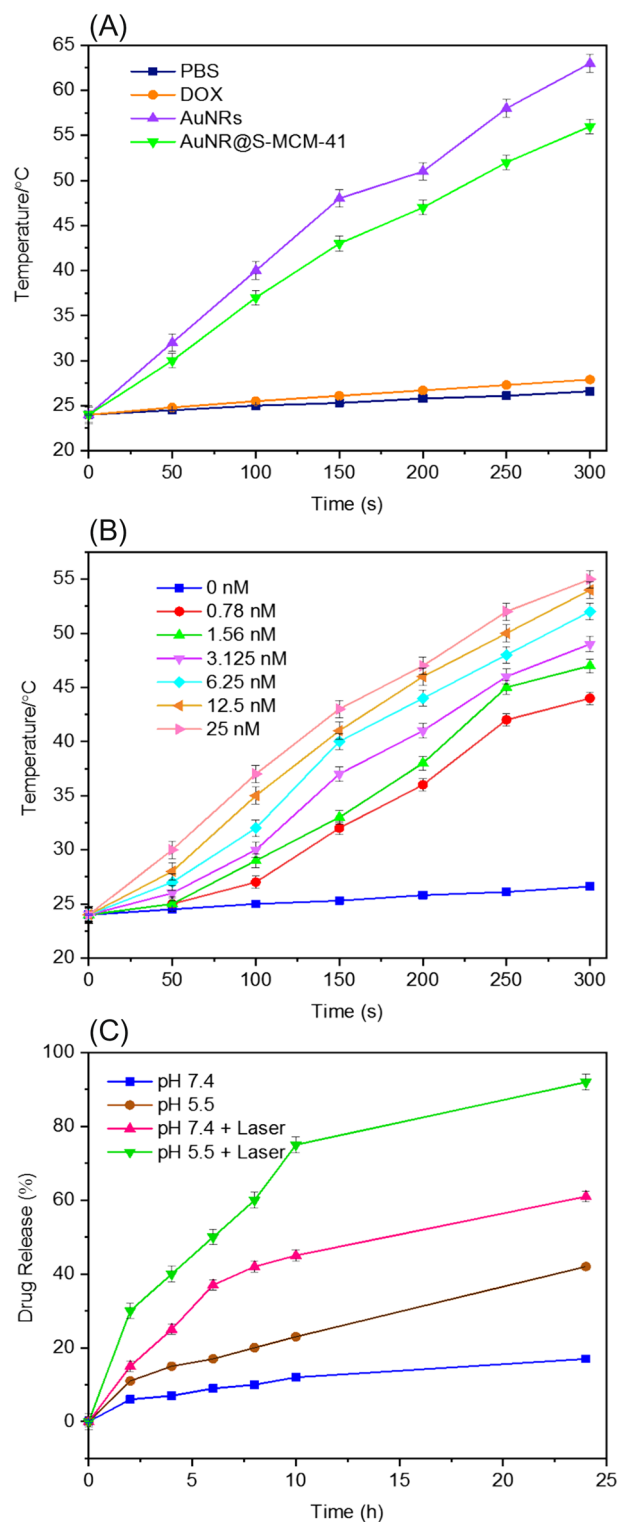


Figure 4. (A) Temperature elevation of PBS, DOX, AuNRs, and AuNR@S-MCM-41 (25 nM AuNR) after irradiating with 808 nm laser intensity (3.6 W cm⁻²); (B) Temperature evolution curves of the solutions containing various concentrations of AuNR@S-MCM-41 (0, 0.78, 1.56, 3.125, 6.25, 12.5 and 25 nM) under NIR laser irradiation with power density of 3.6 W cm⁻². (C) Cumulative DOX release from AuNR@S-MCM-41-DOX in PBS at pH 7.4 and 5.5 without and with NIR irradiation.

for effectively converting light energy to heat energy. Next, the photothermal efficacy of the nanocomposite was evaluated at various concentrations ranging from 0 to 25 nM using NIR laser irradiation (power density of 3.6 W/cm²) (Fig. 4B). The results exhibited a dose-dependent behavior, where the temperature increased with increasing concentrations of AuNRs@S-MCM-41 nanocomposite. Overall, the excellent efficiency of this nanosystem in converting light energy to heat suggests that it can be potentially used as a promising candidate for cancer photothermal therapy.

Anticancer drug loading, entrapment efficiency and release performance

DOX was easily loaded in the AuNR@S-MCM-41 nanocomposite in the phosphate-buffered saline (PBS) solution due to the nanocomposite being mesoporous, and its loading and entrapment efficiency were 26.36 and 48.27 wt%, respectively. As shown in Fig. 4C, the cumulative drug release from the AuNR@S-MCM-41-DOX was studied at pH 7.4 or 5.5 with and without 808 nm laser irradiation. The amount of DOX release from the AuNR@S-MCM-41-DOX was influenced by the pH, leading to the amount of DOX released enhanced with time. It was also found that DOX release in the absence of laser radiation occurs faster at pH 5.5 than pH 7.4. In detail, due to the low solubility of DOX at pH 7.4, AuNR@S-MCM-41-DOX released only 17% of the total loaded DOX in the duration of 24 h. The drug release was increased within 24 h (29%) under acidic conditions at pH 5.5, which is a pH close to the late endosomes and lysosomes in the tumor cell, via protonation of silanol OH groups of AuNR@S-MCM-41-DOX; consequently, the electrostatic bond between the positively charged DOX molecules and the negatively charged of silanol OH groups of AuNR@S-MCM-41-DOX were dissociated. Due to the great solubility of DOX drug at pH 5.5, the release of it was enhanced under these conditions. The pH-triggered drug release performance under the tumor acid intracellular medium can increase the anticancer capability by liberating the drug in tumor cells⁵¹. Compared with our previous work⁴⁶, the DOX release rate in AuNR@SBA-15-SH nanocomposite could reach 32% at pH 5.5. These results revealed that mesoporous silica MCM-41 were efficient in trapping loaded drugs. Also DOX loading and release in AuNR@S-MCM-41 nanocomposite were compared with AuNR@SiO₂-TAT, which was developed using an in situ grafting-cleavage method to modify the bioactive peptide in the core-shell structure of AuNR@SiO₂ for providing synergistic chemo-photothermal cancer treatment. The loading of DOX in AuNR@S-MCM-41 was higher than that in AuNR@SiO₂-TAT (22.5%), and the DOX release rate in AuNR@SiO₂-TAT was 45% at pH 5.5⁵². By contrast, the DOX release behavior of AuNR@S-MCM-41-DOX under 808 nm laser at pH 7.4 exhibited faster DOX release, with the release rate of DOX reaching 61% during 24 h. This difference was ascribed to the photothermal effects of AuNR@S-MCM-41-DOX. NIR laser irradiation provided a localized increase in temperature, which caused the dissociation of weak interactions between DOX and the silanol groups. As the pH of the released solutions reduced to 5.5, DOX release was accelerated, achieving a release rate of 92% with laser irradiation. Reducing pH may contribute to DOX release by weakening the hydrogen bonds and electrostatic binding between DOX and the carrier. Based on these results, the AuNR@S-MCM-41-DOX nanocomposite showed NIR laser and pH dual-responsive DOX drug release behaviors, increasing the efficiency of drug delivery.

Cellular uptake

One of the key requirements for delivering anticancer drugs is the capacity to internalize into cells. ICP-OES spectrometry was used to examine the penetrating effect and consequent localization of AuNR@S-MCM-41-DOX nanocomposites in A549 lung cancer cells.

First, nanocomposites with various concentrations (0.316, 0.632, and 1.265 ppm or 0.78, 1.56, and 3.125 nM) was incubated with A549 cells for 48 h. Then the gold content endocytosed into cells was obtained using ICP-OES spectrometry (0.107, 0.31, and 0.851 ppm). The percentage of internalized Au concentration to the dose of incubated for each cell was measured to determine the cell uptake efficacy by equation (S1). The A549 cells were thoroughly washed with PBS solution before ICP-OES analysis to remove cell-adhered nanocomposites that were not internalized. Consequently, ICP analysis demonstrated the concentration of nanocomposites entering the cells. Following a 48 h incubation period, the internalized amounts of Au atoms per cell were 4.23%, 6.13%, and 8.41%, respectively, indicating that AuNR@S-MCM-41-DOX was uptaken by the cells. This confirms the cell uptake of AuNR@S-MCM-41-DOX in a concentration-dependent manner.

In vitro combined chemo/photothermal therapy Assay

To finally exhibit the near-infrared triggered photothermal-chemo therapy effect of the AuNR@S-MCM-41-DOX nanocomposite on A549 cancer cells, MTT assays were examined under various conditions. It can be seen in Fig. 5A that without irradiation of the 808 nm laser, the AuNR@S-MCM-41 nanoparticles indicated low cytotoxicity to A549 cells at different concentrations (0.39–25 nM). The cell viability was more than 82% after A549 cancer cells were incubated with various concentrations of the AuNR@S-MCM-41 nanocomposite for 48 h. The results exhibited that nanocomposite has good biocompatibility and is relatively nontoxic to cancer cells. When encapsulating DOX into AuNR@S-MCM-41, the treatment effect of AuNR@S-MCM-41-DOX can be changed significantly. The AuNR@S-MCM-41-DOX nanocomposite showed a cell viability of 56% in Fig. 5A, indicating that this nanocomposite indeed performed well in preventing the DOX from leaking. The statistically significant difference between treated cells with concentrations of 12.5 ($p = 0.002698$) and 25 ($p = 0.000003$) AuNR@S-MCM-41 and AuNR@S-MCM-41-DOX in comparison to treated with cells other concentrations were assessed with *t*-test (Fig. 5A). The results in Fig. 5B demonstrated that the viability of cells after treatment with various concentrations of free DOX was 43%. In addition, the results were analyzed and compared to the control group via one-way ANOVA ($p < 0.0001$). Free DOX provided a higher IC₅₀ than the AuNR@S-MCM-41-DOX nanocomposite (at equivalent AuNR concentrations). Therefore, after DOX was loaded in the AuNR@S-MCM-41 nanocomposite, the cell death efficacy in A549 cells through the loading DOX was enhanced (Table 1).

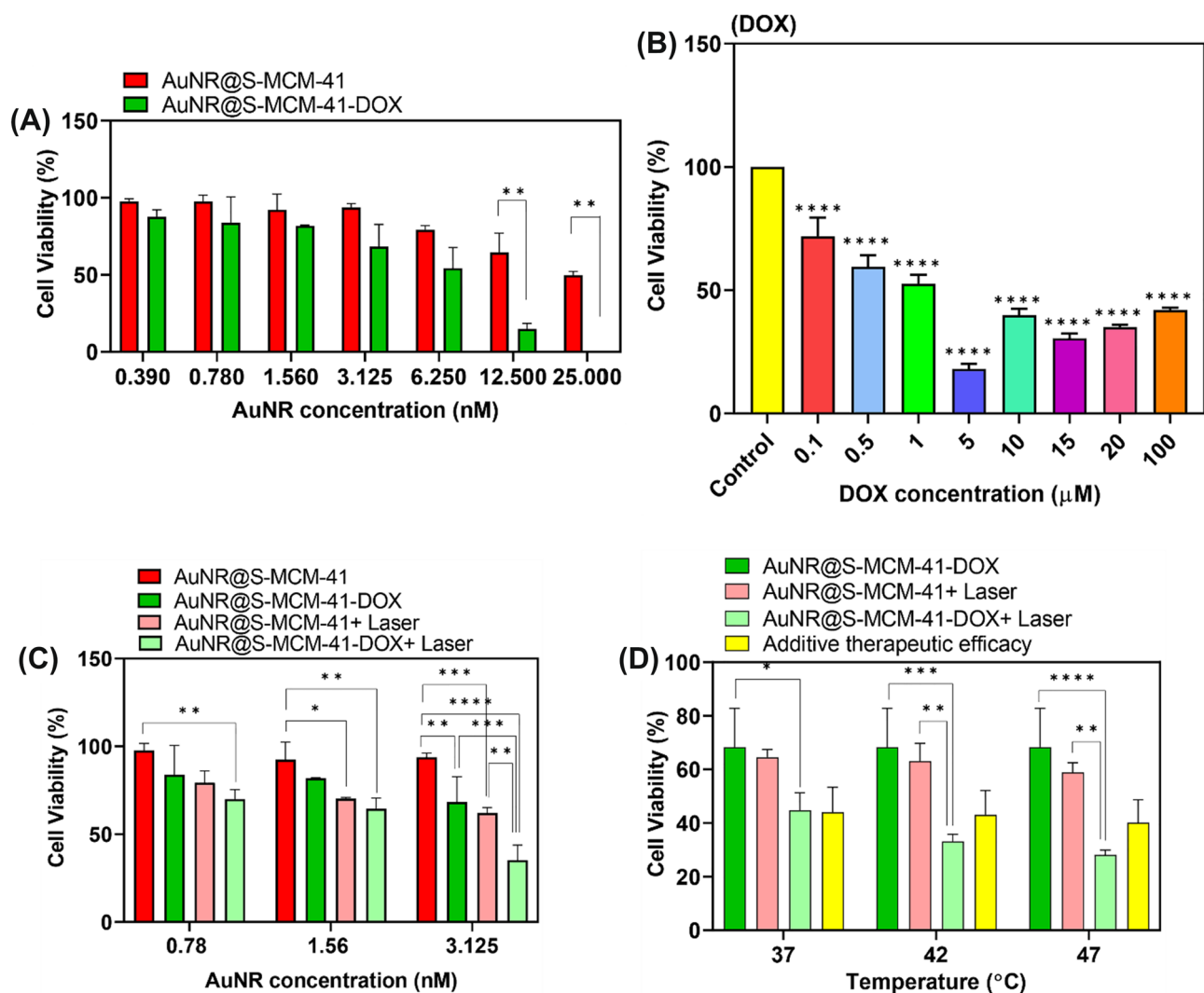


Figure 5. (A) Cell viabilities of the A549 cells after incubation with various concentrations of AuNR@S-MCM-41 and AuNR@S-MCM-41-DOX, (B) free DOX, (C) Comparative cell viabilities of A549 incubated with AuNR@S-MCM-41 or AuNR@S-MCM-41-DOX at different concentrations under exposure to 808 nm laser, (D) A comparison of the viability of the A549 cells treated by AuNR@S-MCM-41 + Laser, AuNR@S-MCM-41-DOX and AuNR@S-MCM-41-DOX + Laser.

AuNR@S-MCM-41	AuNR@S-MCM-41-DOX	Free DOX
7.46 nM	5.3 nM	1.302 μM

Table 1. IC50 of AuNR@S-MCM-41, AuNR@S-MCM-41-DOX and free DOX after 48 h incubation in A549 Cells.

However, after irradiating the cells with an 808 nm laser, the cell viability of cells treated with various concentrations of AuNR@S-MCM-41 dramatically reduced. To assess the therapeutic effect of photothermal therapy, the cells were incubated for 45 h with AuNR@S-MCM-41 at concentrations (AuNRs equivalent 0.78, 1.56 and 3.125 nM). The cell medium was then heated to 37, 42, and 47 °C after 5 min of 808 nm laser irradiation, and the MTT assay was done to examine the therapeutic effect of AuNR@S-MCM-41 + Laser after incubation for 4 h. As seen in Fig. 5C, cell viabilities were negatively correlated with the concentration of the samples. The results exhibited that the AuNR@S-MCM-41 under NIR laser irradiation for 5 min with the dose of 3.125 nM may obviously cause a higher death rate of A549 cells compared with doses of 0.78 and 1.56 nM. These results verified that this nanocomposite has the capability to destroy cancer cells by its great photothermal conversion effect. Conversely, under 808 nm laser irradiation, many cancer cells treated with AuNR@S-MCM-41-DOX died, leading to an improved treatment effect than that of AuNR@S-MCM-41-DOX and AuNR@S-MCM-41 + Laser (Fig. 5C). These findings showed that AuNR@S-MCM-41-DOX can quickly release great amounts of DOX

through its photothermal conversion action, in addition to being able to induce PTT under 808 nm laser irradiation, leading to the final synergistic chemo-photothermal therapy to A549 cells. In comparison to other in vitro experiments, the cell viability of cells treated with AuNRs@S-MCM-41-DOX + Laser was significantly reduced (35% cell viability) after exposure to near-infrared radiation at a dose of 3.125 nM AuNR@S-MCM-41-DOX and a DOX concentration of 0.078 μ M. The results were analyzed by two-way ANOVA control groups. To conclude, there is a synergistic efficacy in the combination therapy in this nanocomposite; the cell viabilities were compared to the determined value from the additive effect. Particularly, the viability of cells of AuNR@S-MCM-41-DOX (in presence and absence of NIR) and AuNR@S-MCM-41 (in presence of NIR) were examined by MTT assay (Fig. 5D), and results were investigated by two-way ANOVA. The gold nanorods concentration in these three groups is 3.125 nM, and DOX concentration is the same (0.078 μ M). After 45 h of incubation with AuNR@S-MCM-41 and AuNR@S-MCM-41-DOX, the cancer cells were exposed to the 808 nm laser and had their media heated to 37, 42, and 47 °C. Furthermore, cells were incubated with AuNR@S-MCM-41-DOX for 48 h, and the viability of cells was 68.2% owing to chemotherapy.

Here, the cell viability of the additive (f_{additive}) was calculated using the relationship $f_{\text{additive}} = f_{\text{chemotherapy}} \times f_{\text{PTT}}$ where f is the cell viability for each treatment. It's an additive effect when $f_{\text{combination}} = f_{\text{additive}}$, but a synergistic effect occurs when $f_{\text{combination}}$ is lower than f_{additive} ⁵³. The experimental cell viability of the combination treatment ($f_{\text{combination}}$) (33.1% at 42 °C and 28.12% at 47 °C) was lower than the computed additive interaction of photothermal therapy and chemotherapy (f_{additive}) (42.98% at 42 °C and 40.1% at 47 °C) of AuNR@S-MCM-41-DOX + Laser, although the results indicated no significant changes in the viability of cells ($p = 0.38, 0.55$). This is expressive of the synergistic anti-cancer efficacy of AuNR@S-MCM-41-DOX + Laser. As shown in Fig. 5D, the increasing therapeutic efficacy of AuNR@S-MCM-41-DOX + Laser was illustrated at temperatures of 42 and 47 compared to 37 °C. The combined chemo-photothermal therapy by AuNR@S-MCM-41-DOX indicated a synergistic effect. The results exhibit that PTT combined with chemotherapy showed an enhanced therapeutic efficacy compared to single chemo- or photothermal therapy.

We tested NIR light-triggered DOX release in cells treated with 0.078 μ M DOX loaded AuNR@S-MCM-41 using 3.6 W/cm² laser power. This showed 35% viability after NIR exposure, indicating efficacious chemo-photothermal therapy. Compared to prior work using 5 μ M DOX and 20 W/cm² laser with Au@SiO₂, our system provides effective therapy at lower drug doses and laser power⁵⁴.

Conclusion

In summary, the AuNR@S-MCM-41-DOX nanocomposite was fabricated as a NIR-activated drug delivery structure for combination chemo-photothermal cancer therapy. This new system has good photothermal conversion performance for efficient photothermal therapy. The resulting nanocomposite indicates pH/NIR dual-responsive drug release performances, and the loaded DOX can be released quickly under an acidic pH environment and NIR stimuli. Cellular uptake studies indicate that the AuNR@S-MCM-41-DOX nanocomposite can be efficiently internalized in A549 lung cancer cells and demonstrates good performance in chemo-photothermal combination therapy to kill cancer cells compared to single chemo- or photothermal therapy. The results of this work indicate that this new nanocomposite has good in vitro biocompatibility and great drug loading capacity, making it a promising candidate for combined chemo-photothermal therapy of lung cancer. These promising results will encourage us to further appraise the in vivo anticancer efficiency of the nanocomposite.

Data availability

All data generated or analysed during this study are included in this published article and its Supplementary Information files.

Received: 4 September 2023; Accepted: 16 February 2024

Published online: 22 February 2024

References

1. Amourizi, F. Z., Malek-Khatibi, A. Z. & Zare-Dorabei, R. Polymeric and composite-based microneedles in drug delivery: Regenerative medicine, microbial infection therapy, and cancer treatment. *Mater. Chem. Horizons* (2023).
2. Sarfjoo, M. R., Shad, A., Hassanpour, M. & Varma, R. An overview on new anticancer drugs approved by food and drug administration: impending economic and environmental challenges. *Mater. Chem. Horizons* **1**, 189–198 (2022).
3. Movagharneshad, N., Ehsanimehr, S. & Najafi-Moghadam, P. Synthesis of poly (N-vinylpyrrolidone)-grafted-magnetite bromoacetylated cellulose via ATRP for drug delivery. *Mater. Chem. Horizons* **1**, 89–98 (2022).
4. Makvandi, P. *et al.* Engineering and development of a tissue model for the evaluation of microneedle penetration ability, drug diffusion, photothermal activity, and ultrasound imaging: A promising surrogate to ex vivo and in vivo tissues. *Adv. Mater.* **35**, 2210034 (2023).
5. Ali, M. R., Wu, Y. & El-Sayed, M. A. Gold-nanoparticle-assisted plasmonic photothermal therapy advances toward clinical application. *J. Phys. Chem. C* **123**, 15375–15393 (2019).
6. Hooshmand, N., Thoutam, A., Anikovskiy, M., Labouta, H. I. & El-Sayed, M. Localized surface plasmon resonance as a tool to study protein corona formation on nanoparticles. *J. Phys. Chem. C* **125**, 24765–24776 (2021).
7. Panikkanvalappil, S. R., Hooshmand, N. & El-Sayed, M. A. Intracellular assembly of nuclear-targeted gold nanosphere enables selective plasmonic photothermal therapy of cancer by shifting their absorption wavelength toward near-infrared region. *Bioconjug. Chem.* **28**, 2452–2460 (2017).
8. Hu, W. C., Younis, M. R., Zhou, Y., Wang, C. & Xia, X. H. In situ fabrication of ultrasmall gold nanoparticles/2D MOFs hybrid as nanozyme for antibacterial therapy. *Small* **16**, 2000553 (2020).
9. Bordley, J. A., Hooshmand, N. & El-Sayed, M. A. The coupling between gold or silver nanocubes in their homo-dimers: A new coupling mechanism at short separation distances. *Nano Lett.* **15**, 3391–3397 (2015).
10. Labouta, H. I., Hooshmand, N., Upreti, T. & El-Sayed, M. A. Localized plasmonic photothermal therapy as a life-saving treatment paradigm for hospitalized COVID-19 patients. *Plasmonics* **16**, 1029–1033 (2021).

11. Rizwan Younis, M., He, G., Gurram, B., Lin, J. & Huang, P. Recent advances in gold nanorods-based cancer theranostics. *Adv. Nanobiomed. Res.* **1**, 2100029 (2021).
12. Sharifi, M. *et al.* Plasmonic gold nanoparticles: Optical manipulation, imaging, drug delivery and therapy. *J. Control. Release* **311**, 170–189 (2019).
13. Falahati, M. *et al.* Gold nanomaterials as key suppliers in biological and chemical sensing, catalysis, and medicine. *Biochim. Biophys. Acta Gen. Subj.* **1864**, 129435 (2020).
14. Song, N. *et al.* Pillar [5] arene-modified gold nanorods as nanocarriers for multi-modal imaging-guided synergistic photodynamic-photothermal therapy. *Adv. Funct. Mater.* **31**, 2009924 (2021).
15. Zhou, R. *et al.* Gold nanorods-based photothermal therapy: interactions between biostructure, nanomaterial, and near-infrared irradiation. *Nanoscale Res. Lett.* **17**, 68 (2022).
16. Ke, L. *et al.* Mitochondria-targeted Ir@ AuNRs as bifunctional therapeutic agents for hypoxia imaging and photothermal therapy. *ChemComm* **55**, 10273–10276 (2019).
17. Li, X. *et al.* In vitro and in vivo photothermal cancer therapeutic effects of gold nanorods modified with mushroom β -glucan. *J. Agric. Food Chem.* **66**, 4091–4098 (2018).
18. Zheng, L. *et al.* Assembly and in vitro assessment of a powerful combination: Aptamer-modified exosomes combined with gold nanorods for effective photothermal therapy. *Nanotechnology* **31**, 485101 (2020).
19. Ngo, D. N. *et al.* Raman thermometry nanopipettes in cancer photothermal therapy. *Anal. Chem.* **94**, 6463–6472 (2022).
20. Chen, J. *et al.* Doxorubicin-conjugated pH-responsive gold nanorods for combined photothermal therapy and chemotherapy of cancer. *Bioact. Mater.* **3**, 347–354 (2018).
21. Patel, U., Rathnayake, K., Singh, N. & Hunt, E. C. Dual targeted delivery of liposomal hybrid gold nano-assembly for enhanced photothermal therapy against lung carcinomas. *ACS Appl. Bio Mater.* **6**, 1915–1933 (2023).
22. Huang, X., Lu, Y., Guo, M., Du, S. & Han, N. Recent strategies for nano-based PTT combined with immunotherapy: From a biomaterial point of view. *Theranostics* **11**, 7546 (2021).
23. Fan, B. *et al.* Photoacoustic-imaging-guided therapy of functionalized melanin nanoparticles: Combination of photothermal ablation and gene therapy against laryngeal squamous cell carcinoma. *Nanoscale* **11**, 6285–6296 (2019).
24. Shang, T., Yu, X., Han, S. & Yang, B. Nanomedicine-based tumor photothermal therapy synergized immunotherapy. *Biomater. Sci.* **8**, 5241–5259 (2020).
25. Zhou, B. *et al.* BSA-bioinspired gold nanorods loaded with immunoadjuvant for the treatment of melanoma by combined photothermal therapy and immunotherapy. *Nanoscale* **10**, 21640–21647 (2018).
26. Licciardi, M. *et al.* In vivo efficacy of verteporfin loaded gold nanorods for combined photothermal/photodynamic colon cancer therapy. *Int. J. Pharm.* **625**, 122134 (2022).
27. de Melo-Diogo, D., Lima-Sousa, R., Alves, C. G. & Correia, I. J. Graphene family nanomaterials for application in cancer combination photothermal therapy. *Biomater. Sci.* **7**, 3534–3551 (2019).
28. Yang, B. *et al.* Super-assembled core-shell mesoporous silica-metal-phenolic network nanoparticles for combinational photothermal therapy and chemotherapy. *Nano Res.* **13**, 1013–1019 (2020).
29. Peltek, O. O. *et al.* Development of nanocarrier-based radionuclide and photothermal therapy in combination with chemotherapy in melanoma cancer treatment. *ACS Appl. Mater. Interfaces* **15**, 13460–13471 (2023).
30. Kadkhoda, J. *et al.* Aptamer-conjugated gold nanoparticles for targeted paclitaxel delivery and photothermal therapy in breast cancer. *J. Drug Deliv. Sci. Technol.* **67**, 102954 (2022).
31. Mukherjee, P., Tripathy, S., Matsabisa, M. G. & Sahu, S. K. Development of upconversion-NMOFs nanocomposite conjugated with gold nanoparticles for NIR light-triggered combinational chemo-photothermal therapy. *J. Photochem. Photobiol. A: Chem.* **437**, 114426 (2023).
32. Raza, F., Zafar, H., Khan, A. U. & Hatami Kahkesh, K. T-cell membrane-coated nanomaterials in cancer treatment. *Mater. Chem. Horizons* **1**, 199–217 (2022).
33. Lopes, J. *et al.* Cell membrane-coated biomaterials for bone cancer-targeted diagnosis and therapy: A critical update on osteosarcoma applications. *Mater. Chem. Horizons* **2**, 65–79 (2023).
34. Huang, R. *et al.* Mesoporous silica nanoparticles: Facile surface functionalization and versatile biomedical applications in oncology. *Acta Biomater.* **116**, 1–15 (2020).
35. Azaroon, M. & Kiasat, A. R. An efficient and new protocol for the Heck reaction using palladium nanoparticle-engineered dibenzo-18-crown-6-ether/MCM-41 nanocomposite in water. *Appl. Organomet. Chem.* **32**, e4271 (2018).
36. Sohrabzadeh, S., Jafarzadeh, A. & Pourahmad, A. Synthesis and characterization of MCM-41 ropes. *Mater. Lett.* **212**, 16–19 (2018).
37. Atiyah, N. A., Albayati, T. M. & Atiya, M. A. Functionalization of mesoporous MCM-41 for the delivery of curcumin as an anti-inflammatory therapy. *Adv. Powder Technol.* **33**, 103417 (2022).
38. Shariatnia, Z. & Pourzadi, N. Designing novel anticancer drug release vehicles based on mesoporous functionalized MCM-41 nanoparticles. *J. Mol. Struct.* **1242**, 130754 (2021).
39. Deaconu, M. *et al.* Tailored doxycycline delivery from MCM-41-type silica carriers. *Chem. Pap* **72**, 1869–1880 (2018).
40. Deaconu, M. *et al.* Exploiting the zwitterionic properties of lomefloxacin to tailor its delivery from functionalized MCM-41 silica. *Microporous Mesoporous Mater.* **305**, 110323 (2020).
41. Dau, T. A. N. *et al.* Surface functionalization of doxorubicin loaded MCM-41 mesoporous silica nanoparticles by 3-aminopropyltriethoxysilane for selective anticancer effect on A549 and A549/DOX cells. *J. Electron. Mater.* **50**, 2932–2939 (2021).
42. Xu, W. *et al.* NIR/pH dual-responsive polysaccharide-encapsulated gold nanorods for enhanced chemo-photothermal therapy of breast cancer. *Mater. Sci. Eng. C* **103**, 109854 (2019).
43. Wang, J. *et al.* Peptide multifunctionalized gold nanorods with dual pH/NIR responsive release of doxorubicin for high-efficiency cancer treatment. *J. Biomed. Nanotechnol.* **15**, 2164–2178 (2019).
44. Liang, Z. *et al.* Gold nanorods@ mesoporous SiO₂@ hyaluronic acid core-shell nanoparticles for controlled drug delivery. *ACS Appl. Nano Mater.* **5**, 7440–7448 (2022).
45. Liu, C., Yang, P., Li, J., Cao, S. & Shi, J. NIR/pH-responsive chitosan hydrogels containing Ti₃C₂/AuNRs with NIR-triggered photothermal effect. *Carbohydr. Polym.* **295**, 119853 (2022).
46. Deinavizadeh, M. *et al.* Smart NIR-light and pH responsive doxorubicin-loaded GNRs@ SBA-15-SH nanocomposite for chemophotothermal therapy of cancer. *Nanophotonics* **10**, 3303–3319 (2021).
47. Deinavizadeh, M. *et al.* NIR/pH dual-responsive DOX-loaded AuNRs@ S- β -CD nanocomposite for highly effective chemophotothermal synergistic therapy against lung cancer cells. *J. Phys. Chem. C* **126**, 18754–18766 (2022).
48. Deinavizadeh, M. *et al.* Near-infrared/pH dual-responsive nanosponges encapsulating gold nanorods for synergistic chemophototherapy of lung cancer. *ACS Appl. Nano Mater.* **6**, 16332–16342 (2023).
49. Guo, K. *et al.* Adsorption of Cs from water on surface-modified MCM-41 mesosilicate. *Water Air Soil Pollut.* **226**, 1–9 (2015).
50. Ashrafizadeh, M. *et al.* Photoactive polymers-decorated Cu-Al layered double hydroxide hexagonal architectures: A potential non-viral vector for photothermal therapy and co-delivery of DOX/pCRISPR. *Chem. Eng. J.* **448**, 137747 (2022).
51. Huang, S.-H. *et al.* Gold nanorods conjugated with biocompatible zwitterionic polypeptide for combined chemo-photothermal therapy of cervical cancer. *Colloids Surf. B* **207**, 112014 (2021).

52. Li, C. *et al.* Mesoporous silica-coated gold nanorods with designable anchor peptides for chemo-photothermal cancer therapy. *ACS Appl. Nano Mater.* **3**, 5070–5078 (2020).
53. Ren, F. *et al.* Gold nanorods carrying paclitaxel for photothermal-chemotherapy of cancer. *Bioconjug. Chem.* **24**, 376–386 (2013).
54. Zhang, Z. *et al.* Mesoporous silica-coated gold nanorods as a light-mediated multifunctional theranostic platform for cancer treatment. *Adv. Mater.* **24**, 1418–1423 (2012).

Acknowledgements

Ali Reza Kiasat acknowledges the support by Center for International Scientific Studies and Collaboration (CISSC).

Author contributions

A.K. conceived and supervised this research. N.H. supervised this research. M.D. performed the experiments and analyzed the data. R.M. and M.S. interpreted the data. M.Sh. performed the Methodology. S.Z. Performed experiments. M.D. and P.M. wrote the main manuscript text. F.K. prepared Figs. 1, 2, 3, 4 and 5. Mi.S. and A.W. revised the manuscript. All authors reviewed the manuscript.

Competing interests

The authors declare no competing interests.

Additional information

Supplementary Information The online version contains supplementary material available at <https://doi.org/10.1038/s41598-024-54778-3>.

Correspondence and requests for materials should be addressed to A.R.K., P.M. or N.H.

Reprints and permissions information is available at www.nature.com/reprints.

Publisher's note Springer Nature remains neutral with regard to jurisdictional claims in published maps and institutional affiliations.



Open Access This article is licensed under a Creative Commons Attribution 4.0 International License, which permits use, sharing, adaptation, distribution and reproduction in any medium or format, as long as you give appropriate credit to the original author(s) and the source, provide a link to the Creative Commons licence, and indicate if changes were made. The images or other third party material in this article are included in the article's Creative Commons licence, unless indicated otherwise in a credit line to the material. If material is not included in the article's Creative Commons licence and your intended use is not permitted by statutory regulation or exceeds the permitted use, you will need to obtain permission directly from the copyright holder. To view a copy of this licence, visit <http://creativecommons.org/licenses/by/4.0/>.

© The Author(s) 2024